Efthimiopoulos, I., Lochbiler, T., Tsurkan, V., Loidl, A., Felea, V., Wang, Y. (2017): Structural Behavior of ZnCr2S4 Spinel under Pressure. - *Journal of Physical Chemistry C*, *121*, 1, pp. 769—777.

DOI: http://doi.org/10.1021/acs.jpcc.6b11253

Structural Behavior of $ZnCr_2S_4$ Spinel under Pressure

I. Efthimiopoulos[1,2], T. Lochbiler[1], V. Tsurkan[3,4], A. Loidl[4], V. Felea[3], and Y. Wang[1*]

[1]*Department of Physics, Oakland University, Rochester, Michigan, 48309, United States*

[2]*Deutsches GeoForschungsZentrum GFZ, Section 4.3, Telegrafenberg, 14473, Potsdam, Germany*

[3]*Institute of Applied Physics, Academy of Sciences of Moldova, MD 2028 Chisinau, Republic of Moldova*

[4]*Experimental Physics 5, Center for Electronic Correlations and Magnetism, Institute of Physics, University of Augsburg, D-86159 Augsburg, Germany*

*E-mail: ywang235@oakland.edu. Phone: (248) 370-3423

Abstract

The series of Cr-chalcogenide spinels ACr_2X_4 (A = Zn, Cd, Hg; X = S, Se) exhibits a rich phase diagram upon compression, as revealed by our recent investigations. There exist, however, some open questions regarding the role of cations in the observed structural transitions. In order to address these queries, we have performed X-ray diffraction and Raman spectroscopic studies on the $ZnCr_2S_4$ spinel up to 42 GPa, chosen mainly due to the similarity of the Zn^{2+} and Cr^{3+} cationic radii. Two reversible structural transitions were identified at 22 and 33 GPa, into a $I4_1/amd$ and an orthorhombic phase, respectively. Close comparison with the behavior of relevant Cr-spinels revealed that the structural transitions are mainly governed by the competition of the magnetic exchange interactions present in these systems, and not by steric effects. In addition, careful inspection of the starting $Fd\bar{3}m$ phase revealed a previously unnoticed *isostructural* transition. The latter is intimately related to changes in the electronic properties of these systems, as evidenced by our Raman studies. Our results provide insights for tuning the physical and chemical properties of these materials, even under moderate compression, as well as promoting the understanding of similar pressure-induced effects in relevant systems.

1. Introduction

The spinel phase (SG $Fd\bar{3}m$, $Z = 8$, **Figure 1**) with a general chemical formula of AB_2X_4 is a versatile host for a variety of transition metal ions[1–3]. The structure comprises of "isolated" tetrahedrally coordinated A cations and octahedrally coordinated B cations. Among the plethora of spinels, the Cr-bearing compounds with nonmagnetic A cations (A = Zn, Cd, Hg) constitute a prototype system for studying magnetic exchange interactions in solids[4–6]. Significant spin-phonon coupling is active in these systems near the magnetic ordering temperatures[7–11], with coupled magneto-structural transitions taking place upon entering the antiferromagnetic (AFM) states for most of these compounds[5,11–14]. Addition to this complexity, several members of this series were reported to exhibit multiferroicity, i.e. manifestation of simultaneous magnetic and ferroelectric ordering[15–19] with intimate structural involvement[11,20,21]. Given this close interrelation between structural, magnetic, and vibrational properties, therefore, variation of the lattice by external pressure provides an appealing method for tuning the physical properties of these systems.

Indeed, several Cr-bearing spinels undergo structural, electronic, and magnetic[22–25] transitions upon sufficient compression. Our recent efforts on the high-pressure behavior on the Cr-based chalcogenide spinels have attempted to elucidate the connection between structural systematics and electro-magnetic ordering in these systems. In particular, our combined experimental and theoretical high-pressure investigations on the $CdCr_2S_4$[26], $CdCr_2Se_4$[27], $HgCr_2S_4$[28], and $HgCr_2Se_4$[29] compounds unraveled a similar structural trend under pressure, with successive transitions toward tetragonal and orthorhombic phases. However, $ZnCr_2Se_4$ exhibits a rather distinct high-pressure behavior, adopting a monoclinic structure starting at 17 GPa[30]. The latter is a superstructure of the well-known Cr_3S_4-type phase, a common high-pressure and high-

temperature polymorph for Cr-based sulfide and selenide spinels[23,25,31,32]. A plausible explanation behind this cubic-monoclinic transition in $ZnCr_2Se_4$ and, hence, its diverging structural behavior, might stem from the similarity in the cationic radii of Zn^{2+} and Cr^{3+} [$r(Zn^{2+})^{IV}$ = 0.6 Å; $r(Cr^{3+})^{VI}$ = 0.615 Å][33], which may in turn facilitate such structural transformation.

In order to explore this scenario, we have investigated the high-pressure structural and vibrational properties of the relevant $ZnCr_2S_4$ spinel. This material undergoes two successive magneto-structural transitions at 15 K (SG $I4_1/amd$, Z = 4) and at 8 K (SG *Imma*, Z = 4) at ambient pressure, with both phases exhibiting antiferromagnetic (AFM) ordering[12]. There have been three reports on the effect of pressure on the magnetic and structural properties of $ZnCr_2S_4$ to date[34–36]. More precisely, pressure enhances the AFM interactions in $ZnCr_2S_4$, consistent with the behavior of other Cr-based spinels upon compression[37,38]. In addition, a previous X-ray diffraction (XRD) study indicated the onset of amorphorization beyond 10 GPa[36]. In light of our recent findings on similar Cr-bearing chalcogenide spinels, however, the pressure-induced structural evolution of $ZnCr_2S_4$ calls for a re-examination.

Indeed, our high-pressure XRD and Raman spectroscopic investigations on $ZnCr_2S_4$ up to 42 GPa revealed two reversible structural transitions at 22 GPa, into a tetragonal $I4_1/amd$ phase, whereas an orthorhombic phase was detected at ~33 GPa. Overall, $ZnCr_2S_4$ closely resembles the structural trend of the $CdCr_2S_4$[26], $CdCr_2Se_4$[27], $HgCr_2S_4$[28], and $HgCr_2Se_4$[29] compounds, hence excluding the similarity in the cationic radii of Zn^{2+} and Cr^{3+} as the reason behind the structural divergence of $ZnCr_2Se_4$[30].

Following our previous proposal[27], we detected a direct link between the $Fd\bar{3}m \rightarrow I4_1/amd$ transition pressure and the ratio of magnetic exchange interactions active in these systems.

Consequently, it appears that the tuning of the magnetic properties by external pressure can lead to structural transitions toward phases of lower crystalline symmetry, i.e., sufficient compression is able to induce spin-driven Jahn-Teller transitions in these systems. Interestingly, $ZnCr_2Se_4$ does not fit into the aforementioned linear trend, indicating that the cubic-monoclinic transition is most likely originating from distinct magnetic effects active in $ZnCr_2Se_4$.

Finally, careful analysis of the $Fd\bar{3}m$ structural parameters for $ZnCr_2S_4$ revealed a previously unnoticed *isostructural* transition taking place between 9 and 14 GPa. This isostructural transition appears to be related to changes in the electronic properties of this system. The latter is evidenced for example by an abrupt drop of the overall Raman intensity, a common trend among Cr-bearing chalcogenide spinels under pressure[26–30]. Similar coupled isostructural-electronic transitions were also discovered for the $HgCr_2S_4$ and $ZnCr_2Se_4$ compounds, within the stability region of the ambient-pressure $Fd\bar{3}m$ phase.

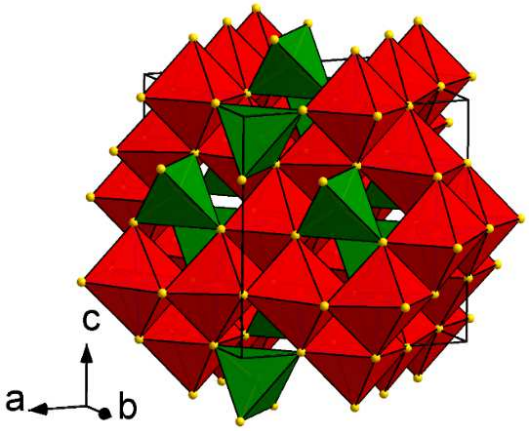

Figure 1. Polyhedral representation of the spinel structure (SG $Fd\bar{3}m$, Z = 8). The green tetrahedra correspond to ZnS_4 units, whereas the red octahedra represent the CrS_6 cages, with the Zn and Cr cations residing in the respective polyhedral units. The S ions are displayed as yellow spheres.

2. Experimental Section

Details of the $ZnCr_2S_4$ sample synthesis have been reported elsewhere[12,39]. High pressure measurements were carried out by using a rhenium gasketed diamond anvil cell (DAC), equipped with a set of diamonds with 300 μm culet size. The ruby luminescence method was employed for pressure calibration[40].

The angle-resolved high-pressure powder XRD measurements at room temperature were performed at the 16BM-D beamline of the High Pressure Collaborative Access Team, at the Advanved Photon Source of Argonne National Laboratory. The incident monochromatic X-ray beam energy was E = 29.2 keV (λ = 0.4246 Å), and the sample-detector distance was 318 mm. Helium served as pressure transmitting medium (PTM). The measured XRD diffractograms were processed with the FIT2D software[41]. Refinements were performed using the GSAS+EXPGUI software packages[42,43]. The *P-V* data were fitted with a Birch-Murnaghan equation of state (B-M EoS)[44] using the EosFit program[45].

High-pressure Raman experiments at room temperature were conducted on single-crystalline $ZnCr_2S_4$ samples with a solid-state laser (λ = 532 nm), coupled with a single-stage Raman spectrometer (Andor S500i) and a charge-coupled device. Both helium and a mixture of methanol-ethanol-water (M/E/W) 16:3:1 served as PTM in separate runs, yielding similar results. The Raman spectra were calibrated with a Hg lamp.

3. Results and discussion

3.1. Structural Properties under Pressure

In order to characterize the pressure-induced structural evolution of $ZnCr_2S_4$, we have conducted *in situ* high-pressure XRD studies. Selected XRD patterns are presented in **Figure 2**. We can observe that the initial $Fd\bar{3}m$ phase persists up to ~20 GPa. New Bragg features appear

at 21 GPa, indicative of a structural transformation at that pressure. The XRD patterns are dominated by the new high-pressure phase at ~23 GPa already.

The majority of the Bragg peaks for this first high-pressure phase could be indexed to a tetragonal $I4_1/amd$ structure (Z = 4), a common high-pressure modification for Cr-based spinels[28–30]. We note that the SG $I4_1/amd$ is a direct subgroup of SG $Fd\bar{3}m$[46], with the c-axis in the two structures being common, whereas the tetragonal a_{tetr}-axis equals the cubic lattice parameter a_{cub} divided by $2^{1/2}$ (we employ the normalized $a^* = a_{tetr}\sqrt{2}$ tetragonal lattice parameter in our discussion from now on, for direct comparison with a_{cub}); in addition, both phases exhibit the same cationic coordination, i.e. 4-fold for Zn and 6-fold for Cr.

Increasing pressure further leads to a splitting of several tetragonal Bragg peaks at ~33 GPa [e.g. the (200) Bragg peak at ~7^o in **Figure S1 in Supporting Information**], thus signifying another structural transition. This second high-pressure phase could be assigned to an orthorhombic distortion of the tetragonal cell, consistent with the pressure-induced behavior of relevant Cr-spinels[26,28]. Given the preferred orientation and the broadening of the Bragg peaks, however, an unambiguous space group assignment was not feasible in this case. For performing the XRD refinements, however, we have employed SG *Imma* due to the following reasons: (a) it is a direct subgroup of SG $I4_1/amd$, hence the cationic coordination is retained, and (b) it is a low-temperature modification of $ZnCr_2S_4$, which undergoes a similar sequence of structural transitions, i.e., cubic→ tetragonal→orthorhombic upon lowering temperature[12]. Furthermore, the $Fd\bar{3}m$ phase is recovered upon decompression, consistent with the general trend of Cr-spinels[26,28–30,47].

We should mention, however, that neither the tetragonal $I4_1/amd$ nor the orthorhombic high-pressure $ZnCr_2S_4$ modifications could reproduce all of the observed peaks, with (at least) four

Bragg features in the former and six peaks in the latter case escaping indexing (asterisks in **Figure 2 & Figure S2 in Supporting Information**). At first, we attempted to index the first high-pressure phase assuming another (single) structural model. Among the plausible structural candidates, we considered (a) a monoclinic Cr_3S_4-type structure (SG $C2/m$, $Z = 2$), which is the high-pressure phase of $FeCr_2S_4$[22] and a common high-pressure and high-temperature polymorph for several sulfide spinels[31], (b) a $CrMo_2S_4$-type structure (SG Cc, $Z = 8$), a superstructure of the aforementioned Cr_3S_4[48] and the high-pressure phase of $ZnCr_2Se_4$[30], (c) the two monoclinic high-pressure structures reported for Co_3O_4[49], and (d) the denser $CaTi_2O_4$-, $CaFe_2O_4$-, and $CaMn_2O_4$-type orthorhombic phases adopted by spinel oxides upon sufficient compression[50,51]. None of these phases, however, could reproduce all of the observed Bragg features.

Consequently we checked for possible impurities that may arise after the first structural transition of $ZnCr_2S_4$ due to e.g. partial decomposition, as predicted for Cr-based oxide spinels[52]. Even though we can probably exclude utter decomposition of $ZnCr_2S_4$ into its binary constituents ZnS and Cr_2S_3 and/or elemental dissociation, since the original spinel phase is recovered upon decompression [**Figure 2**], partial dissociation may still be a viable possibility. However, neither a combination of rocksalt-type ZnS[53] and the high-pressure modification of Cr_2S_3[54], nor elemental Zn[55] and any sulfur polymorphs stable in this P-T range (S-I and S-II[56,57]) could be detected in our XRD patterns. Furthermore, the contamination of our XRD patterns from external sources such as the ruby pressure marker, the rhenium gasket material, and/or helium (PTM) was also tested and excluded. Hence, we conclude that the $ZnCr_2S_4$ XRD patterns above 21 GPa are composed of a phase mixture, respectively, with the primary phase being the tetragonal $I4_1/amd$ phase (22-30 GPa) and its orthorhombic distortion (30-42 GPa). The secondary minority phase (or phases) could not be identified at this stage due to the limited

number of Bragg peaks available for indexing. It is also not clear at this point whether these 'secondary' Bragg features in the $I4_1/amd$ and orthorhombic XRD patterns correspond to the same structure (**Figure S3 in Supporting Information**).

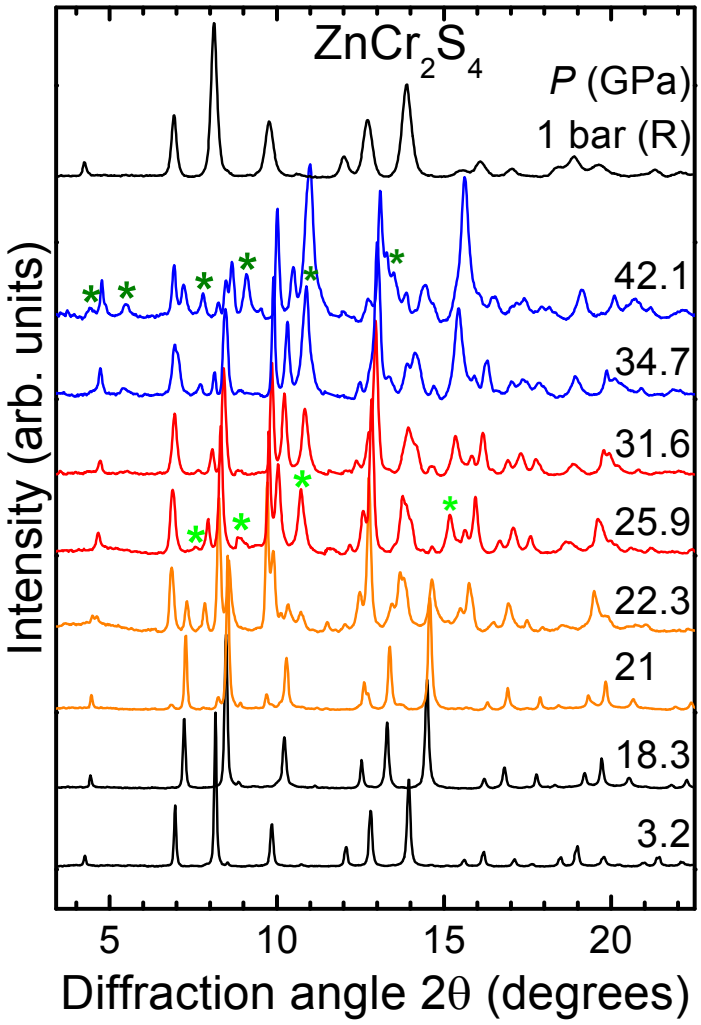

Figure 2. Selected XRD patterns of $ZnCr_2S_4$ at various pressures (T = 300 K, λ = 0.4246 Å). The various phases are indicated by black ($Fd\bar{3}m$), red ($I4_1/amd$), blue ($Imma$), and orange (phase mixture). Asterisks mark the strongest Bragg peaks of the secondary phase(s) (see text).

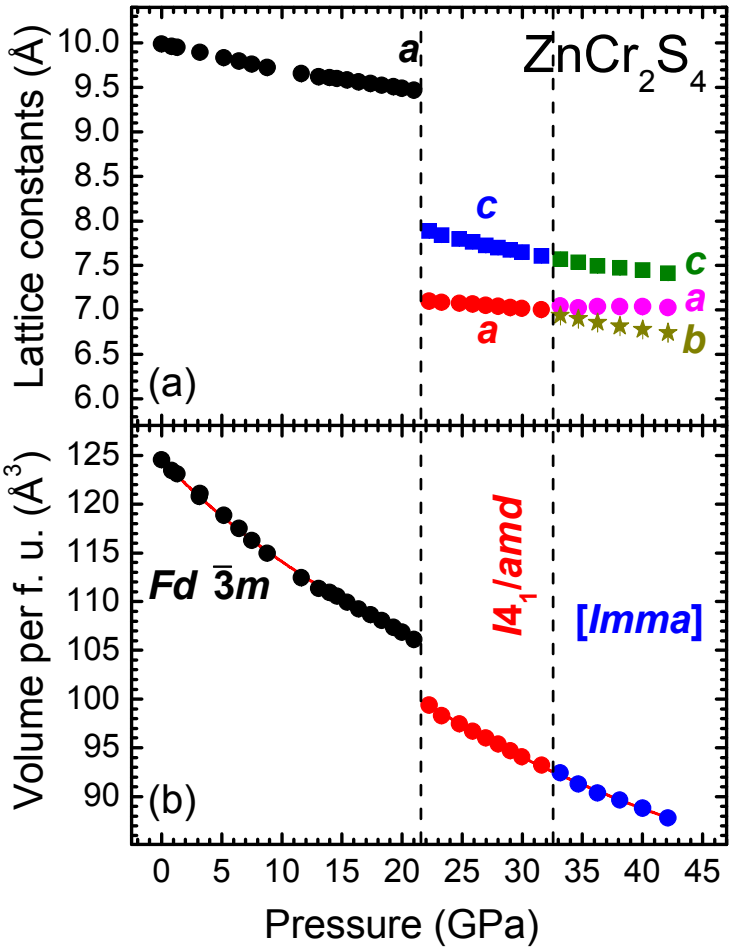

Figure 3. (a) Lattice constants and (b) unit cell volume per formula unit as a function of pressure for the various phases of $ZnCr_2S_4$. Error bars lie within the symbols. The vertical dashed lines mark the onset pressures of the structural transitions, whereas the red solid line represents the fitted Birch-Murnaghan EoS functions.

Turning now to the evolution of the structural parameters under pressure, we note that the quality of the obtained XRD diffractograms allowed for full Rietveld refinements of the $Fd\bar{3}m$ and the $I4_1/amd$ structures (**Table S1 in Supporting Information**). However, only the lattice parameters could be extracted for the orthorhombic phase. In **Figure 3** we plot the pressure-induced behavior of the lattice parameters and the respective volumes for all of the $ZnCr_2S_4$

phases. The fitting of the $Fd\bar{3}m$ *P-V* data with a third-order B-M EoS yielded a bulk modulus value of B_0 = 96(3) GPa (**Table 1**), consistent with the bulk moduli of relevant Cr-spinels[28–30,58,59] and almost identical with the previous XRD study conducted up to 12 GPa[36]. Upon passing into the tetragonal phase, we notice a sizable volume change at the transition point (~5%, **Figure 3**). Inspection of the lattice parameters reveals that the volume drop is primarily attributed to the small $c/a^* < 1$ tetragonal axial ratio (**Table S1 in Supporting Information**). Even though similar first-order $Fd\bar{3}m$ – $I4_1/amd$ transitions have been observed for other spinels under pressure[60,61], the volume change at the transition point cannot be rationalized by SG symmetry considerations alone[46]. We discuss this point in more detail below.

Table 1. Elastic Parameters (Volume Per Formula Unit V_{Tr} / Z, the Bulk Modulus B_{Tr}, and the Pressure Derivative of Bulk Modulus B'_{Tr}) for the Various Phases of $ZnCr_2S_4$ under Pressure, As Obtained by the Fitting of Birch-Murnaghan EoS Forms[44] to the Measured *P-V* Data[a].

Phase	P_R (GPa)	V_R / Z (Å^3)	B_R (GPa)	B'_R
$Fd\bar{3}m$	10^{-4}	124.6(exp.)	96(3)	4.3(4)
$I4_1/amd$	22.3	99.5 (exp.)	125(2)	4(fixed)
[*Imma*]	33.2	92.4 (exp.)	153(4)	4(fixed)

[a]Each parameter is evaluated at a reference pressure P_R. Exp.= experimental value.

Finally, the $I4_1/amd$ – orthorhombic transition does not exhibit any visible volume change at the transition point; the tetragonal and orthorhombic *c*-axis exhibiting a rather continuous transition, whereas the tetragonal *a*-axis splits into an (almost) incompressible orthorhombic *a*-axis and a more compressible *b*-axis (**Figure 3**). The ‘‘orthorhombicity’’, i.e., the *b*/*a* ratio deviates more than unity upon further compression. Overall, the $I4_1/amd$ – orthorhombic transition can be classified as a second-order transition. Both the $I4_1/amd$ and the orthorhombic

P-V data could be described with a single (second-order) B-M EoS form [**Figure 3(b) & Table 1**].

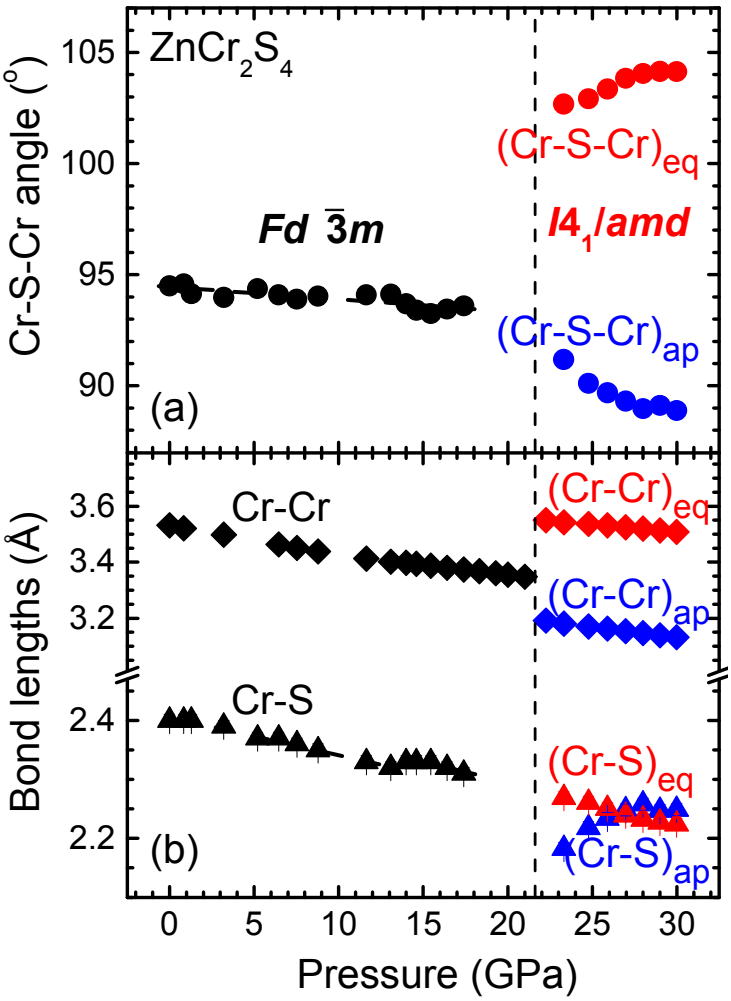

Figure 4. Pressure-induced changes of (a) the Cr-S-Cr bond angles and (b) the Cr-S, and Cr-Cr bond lengths for the $Fd\bar{3}m$ and the $I4_1/amd$ phases.

In order to get a more comprehensive understanding of the cubic-tetragonal transition, we turn now to the evolution of the interatomic parameters against pressure. Selected bond angles and bond lengths are shown in **Figure 4**. The Cr-S-Cr bond angle, which serves as the pathway for the nn FM superexchange in the $Fd\bar{3}m$ phase[4,6], exhibits a marginal decrease against pressure [**Figure 4(a)**]. This appears to be a common feature among Cr-based spinels[28,29,60,61].

Furthermore, all of the cation-anion bond distances decrease upon compression, with the Zn-S bond being slightly more compressible (**Table S1 & Figure S5 in Supporting Information**). Upon passing into the $I4_1/amd$ phase, the Cr-S-Cr, Cr-S, and Cr-Cr parameters split into two components due to the tetragonal symmetry, into an apical (along *c*-axis) and an equatorial (parallel to *ab*-plane) constituent; however, the Zn-S bond distance remains unique (**Figure 4 & Table S1 in Supporting Information**). The shortened Cr-S (and Cr-Cr) bond distances along the apical direction indicate a 'flattening' of the CrS_6 octahedra along the respective axis, implying significant changes in the corresponding magnetic exchange interactions. We finally mention the expansion of the Zn-S bond length upon the $Fd\bar{3}m$ – $I4_1/amd$ transition, partially compensating for the shortening of the apical Cr-S bonds (**Table S1 in Supporting Information**).

3.2. High-Pressure Raman Spectroscopy

Having established the structural sequence of $ZnCr_2S_4$ from our XRD investigation, we turn now to our Raman spectroscopic studies. As we explain below, except from the detection of the high-pressure phases, we could additionally resolve an electronic transition taking place in the $Fd\bar{3}m$ phase.

For the starting $Fd\bar{3}m$ phase of $ZnCr_2S_4$, we observed all of the five expected Raman bands (**Figure 5**)[62,63];. The measured zero-pressure frequencies ω_0 (**Table S4 in Supporting Information**) are in good agreement with the previously reported values[62,63]. All of the $Fd\bar{3}m$ bands exhibit normal behavior upon compression, i.e. their frequencies increase against pressure (**Figure 5b**).

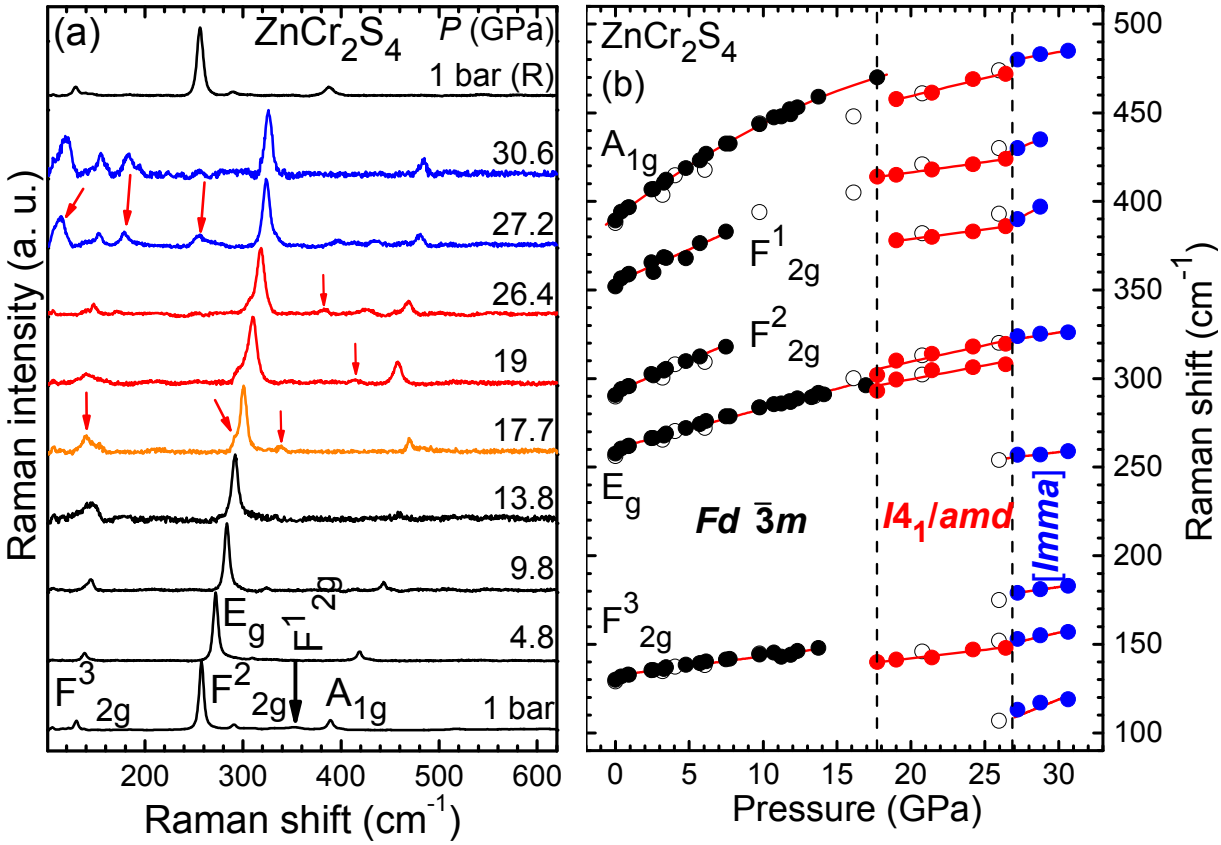

Figure 5. (a) Normalized Raman spectra of $ZnCr_2S_4$ at selected pressures (λ = 532 nm, T = 300 K). The various phases are indicated by different colors: black for $Fd\bar{3}m$, red for $I4_1/amd$, blue for orthorhombic, and orange for coexistence. Arrows denote the new Raman-related features. Background has been subtracted for clarity. (b) Raman mode frequency evolution against pressure. Closed and open symbols depict measurements upon increasing and decreasing pressure, respectively. The vertical dashed lines represent the onset of the phase transitions.

The $Fd\bar{3}m$ Raman-active modes are retained up to ~18 GPa (**Figure 5a)**. Beyond that pressure, we observe a total of five new Raman-active modes in the Raman spectra, such as the low-frequency sideband at ~290 cm^{-1} of the strongest E_g peak. The appearance of these novel Raman features indicate a pressure-induced structural transition of the $Fd\bar{3}m$ phase close to 18 GPa, in

very good agreement with our XRD results. Interestingly, we note that the low-frequency F^3_{2g} and the high-frequency A_{1g} modes, which appear to 'persist' in the high-pressure phase, exhibit an abrupt frequency drop at the structural transition point (**Figure 5b)**. Finally, we note that the overall Raman intensity of $ZnCr_2S_4$ showed a substantial reduction in the vicinity of the transition point. Close examination of the spectra revealed that the Raman intensity drops abruptly *prior* to this first pressure-induced transition, i.e. close to ~11 GPa. We will come back to this point later.

Our XRD study has identified this first high-pressure phase as a $I4_1/amd$ structure. According to group theory, a sum of ten Raman-active modes are expected for this tetragonal phase[64]. Due to the overall low Raman intensity after the transition, however, only six Raman bands can be resolved (**Figure 5**). The two most prominent features of the $I4_1/amd$ phase are expected to result from the splitting of the $Fd\bar{3}m$ E_g mode[64], consistent with our observations. As for the frequency reduction of the A_{1g} stretching mode upon the $Fd\bar{3}m \rightarrow I4_1/amd$ transition, it can be rationalized by the Cr-S bond length asymmetry induced by transforming into the tetragonal phase, i.e. the splitting of the Cr-S bond lengths into two distinct and unequal values[65] (**Figure 4b)**.

Upon further pressure increase, we can observe additional changes in the Raman spectra at ~27 GPa (**Figure 5**). In particular, three new Raman features appear within the 100-300 cm^{-1} frequency range, whereas the "descendant" of the $Fd\bar{3}m$ E_g mode and its sideband merge again in a single peak above 27 GPa. This behavior hints another pressure-induced transition in $ZnCr_2S_4$ close to that pressure, consistent with the $I4_1/amd$-orthorhombic transition evidenced in our XRD results. Finally, the starting $Fd\bar{3}m$ phase is recovered upon decompression, again in agreement with the XRD studies (**Figure 5**).

Before closing the **section**, we note that the transition pressures P_{Tr} of the $Fd\bar{3}m \rightarrow I4_1/amd$ and the $I4_1/amd \rightarrow$orthorhombic transitions determined by our XRD study are 3-6 GPa higher compared to our Raman observations. The minor deviations in the P_{Tr} can be accounted for by (a) the different PTM employed in the two investigations[66,67] (M/E/W remains hydrostatic up to ~10.5 GPa, whereas helium provides generally good hydrostatic conditions up to 40 GPa)[68], (b) the use of different types of sample in the two studies (powder for XRD, single crystals for Raman), and (c) the different ''sensitivity'' of the two methods (Raman probes the structure on a local scale, whereas XRD serves as a more bulk probe of the lattice). Since the Raman investigations were performed with both PTM and yielded almost identical results, we tend to attribute the small P_{Tr} differences in the different form of samples used in the two studies and the more local nature of Raman spectroscopy (see e.g. Ref.69 for more details).

3.3. Comparison with Relevant Cr-Spinels

The pressure-induced sequence of cubic-tetragonal-orthorhombic structural transitions observed in $ZnCr_2S_4$ is consistent with the structural trends of most Cr-bearing chalcogenide spinels upon compression (**Figure 6**)[26–30], as well as with the structural sequence reported for $ZnCr_2S_4$ at ambient pressure and low temperatures[12]. Our results, however, clearly contradict the previous high-pressure $ZnCr_2S_4$ single-crystal XRD investigation of Wittlinger *et al.*[36], where the onset of amorphization around 10 GPa was reported. Even though the reasons for this discrepancy are not clear, we can offer some plausible reasons such as (1) the different PTM in the two studies, i.e. we used helium compared to the argon and alcohol mixture used by Wittlinger *et al.*[36], (2) possible pressure-induced texture effects in the single-crystal XRD study, and (3) it is not clear whether the $ZnCr_2S_4$ sample of Wittlinger *et al.*[36] was synthesized in a

similar way to our samples, since the synthesis procedure may alter the respective properties[3]. Nevertheless, an up-to-date single-crystal XRD investigation on $ZnCr_2S_4$ is required to fully resolve this issue.

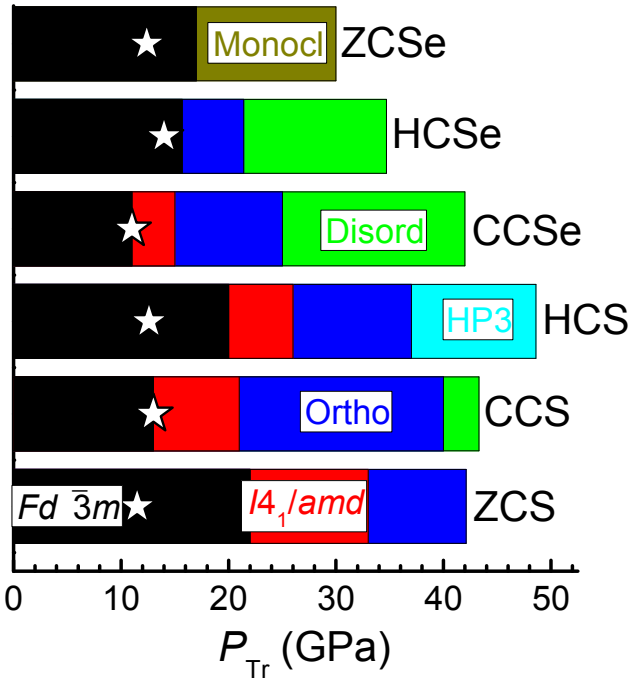

Figure 6. Overview of the pressure-induced structural behavior for several Cr-based spinels at ambient temperature. The stability field for each phase is indicated with a different color: black for the starting $Fd\bar{3}m$, red for $I4_1/amd$, blue for orthorhombic, green for disorder, cyan for an unidentified high-pressure phase (HP3), and yellow for the $CrMo_2S_4$-type. The open star symbols denote the onset of the Raman intensity drop. Abbreviations: ZCS = $ZnCr_2S_4$, CCS = $CdCr_2S_4$, HCS = $HgCr_2S_4$, CCSe = $CdCr_2Se_4$, HCSe = $HgCr_2Se_4$, and ZCSe = $ZnCr_2Se_4$. Data are from Refs.26–30.

Except from the high-pressure structural behavior, another common trend for the Cr-bearing spinels is a potential pressure-induced insulator-metal transition. This electronic modification is evidenced by (a) an overall Raman intensity drop (**Figure 7a**)[26–30], (b) mid-infrared

reflectance[26,70], and (c) theoretical predictions[71]. In **Figure 6** we have marked the onset pressures for this electronic change P_{el} for all of the relevant Cr-spinels, as evidenced by the overall Raman intensity reduction (we chose this method for determining P_{el}, since it represents a complete data set for these compounds). It becomes apparent that P_{el} appears to be independent of the Cr-spinel composition. Even though P_{el} lies in the vicinity of the first pressure-induced structural transition for half of these materials, thus not being certain whether the electronic transition is simply a byproduct of the structural transformation, in the $ZnCr_2S_4$, $ZnCr_2Se_4$, and $HgCr_2S_4$ compounds the two effects seem decoupled, i.e., the electronic transition takes place within the stability range of the starting $Fd\bar{3}m$ structure in the latter materials.

In order to look for subtle structural changes which may reflect the aforementioned electronic change, we have employed the Eulerian strain f_E as a function of the normalized pressure F (F-f_E) plots[45] for the $ZnCr_2S_4$, $ZnCr_2Se_4$, and $HgCr_2S_4$ compounds. This approach has served well before for identifying subtle structural anomalies in the vicinity of electronic transitions[72,73]; the F-f_E parameters should exhibit a linear correlation, with potential divergence from a linear trend implying (subtle) structural changes. Plotting of the F-f_E parameters reveals a break between 9 and 14 GPa for $ZnCr_2S_4$, and 8-11 GPa for both $HgCr_2S_4$ and $ZnCr_2Se_4$ (**Figure 7b)**, in excellent agreement with the P_{el} values determined from Raman spectroscopy (**Figure 6**). Hence, we can conclude that the pressure-induced electronic transition in the $ZnCr_2S_4$, $ZnCr_2Se_4$, and $HgCr_2S_4$ spinels is accompanied by a previously unnoticed subtle *isostructural* transition. For the remaining compounds, the electronic transition roughly coincides with the $Fd\bar{3}m$ – $I4_1/amd$ structural change as we mentioned before, hence becoming difficult to determine if such isostructural transitions are a general feature of this series. Interestingly, we note that a *peculiar* F-f_E plot was recently reported for the $Fd\bar{3}m$ phase of a natural $CuCr_{1.7}V_{0.03}S_4$ sample[74]. Even

though this behavior was attributed to a unique signature of a fourth-order B-M EoS for describing the respective *P-V* data, it would be interesting to check whether an isostructural/electronic transition is also at play in this system.

In order to gain a microscopic understanding of the isostructural transition mechanism in $ZnCr_2S_4$, we took a closer look of the interatomic parameters between 9 and 14 GPa. Close examination of these parameters revealed subtle changes in the Zn-S and Cr-S bond distances (**Figure S5 in Supporting Information**). In particular, the Cr-S bond expands and the Zn-S bond contracts in the vicinity of the isostructural transition, with both bond distances becoming (within error) incompressible after the transition; a slight drop was also observed in the Cr-S-Cr bond angle. Since these parameters modulate the charge transfer among the cations[4], a possible explanation behind the concomitant electronic and isostructural transition might be some partial charge transfer from e.g. the anions toward the cations at that pressure. Since the electronic transition does not appear to depend on either the divalent A cation (Zn, Cd, Hg) or the anion (**Figure 6**), it should originate mainly from the Cr^{3+} cations sitting at the octahedral sites of the spinel structure (**Figure 1**). More suitable microscopic probes are needed to elucidate the exact mechanism of these changes.

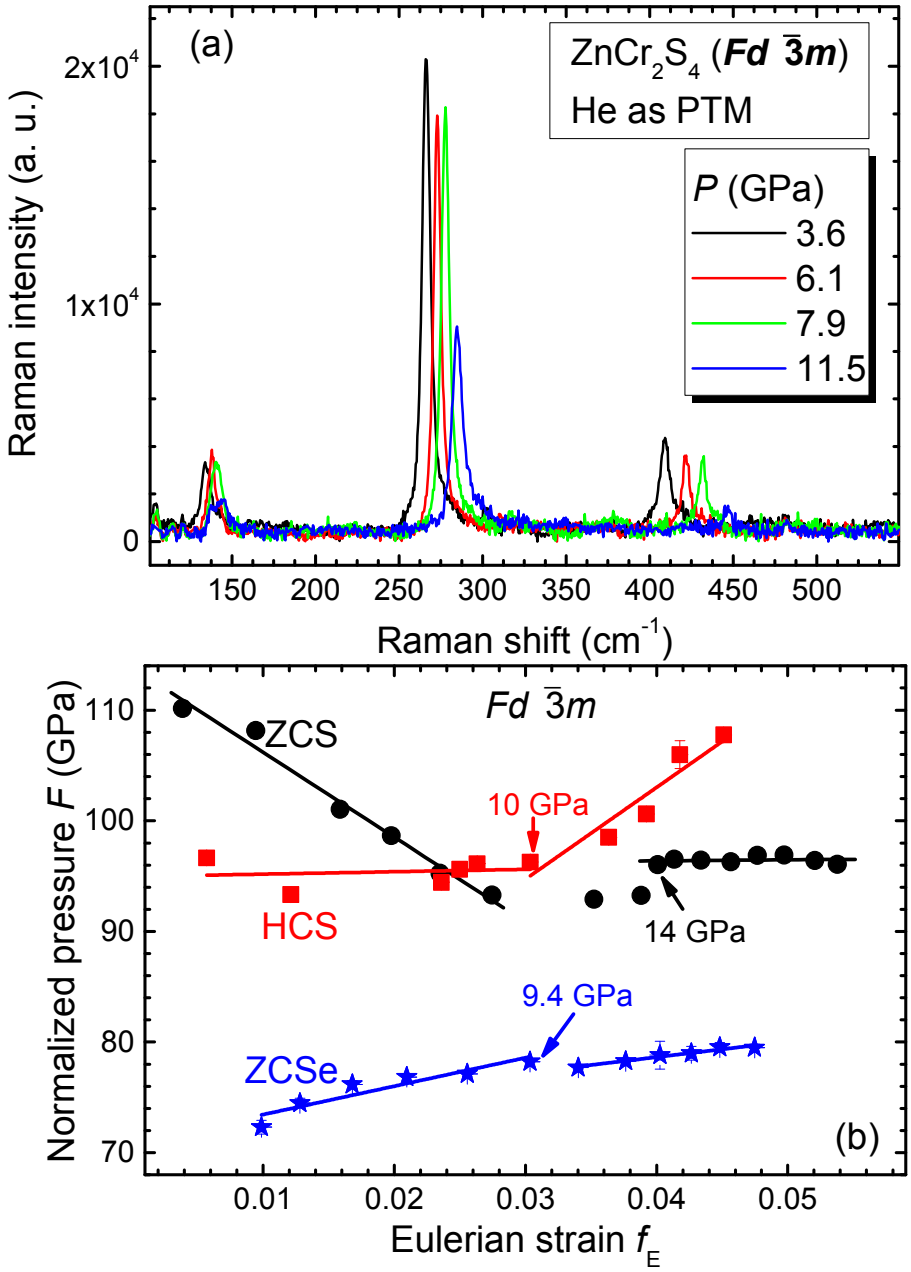

Figure 7. (a) As-measured Raman spectra of the $ZnCr_2S_4$ $Fd\bar{3}m$ phase at selected pressures (He as PTM). Notice the Raman intensity reduction above 8 GPa, prior to the $Fd\bar{3}m \rightarrow I4_1/amd$ transition. (b) Plot of the normalized stress F as a function of the Eulerian strain f_E for the $Fd\bar{3}m$ phases of $ZnCr_2S_4$ (black), $HgCr_2S_4$ (red), and $ZnCr_2Se_4$ (blue). The fitting parameters are listed in **Table S3 in Supporting Information**. Data are from Refs.28 and 30.

Another common feature of these systems is the noticeable volume change at the $Fd\bar{3}m \rightarrow I4_1/amd$ transition point[28,29,60,61], which is unexpected from group symmetry considerations. Following our previous discussion on $CdCr_2Se_4$[27], we focus on the magnetic exchange interactions of $ZnCr_2S_4$. In **Figure 8** we plot the ratio of the nearest-neighbor (nn) J and the next-nearest-neighbor (nnn) K as a function of the $Fd\bar{3}m \rightarrow I4_1/amd$ transition pressure P_{Tetr} (**Table S2 in Supporting Information**). As we can clearly observe, there is a linear trend between the K / J ratio and the corresponding P_{Tetr} for all of the Cr-bearing chalcogenide spinels which exhibit the $Fd\bar{3}m \rightarrow I4_1/amd$ transition. This observation is in line with the earlier discussion[27], and hints the crucial role of the (initially weaker) nnn interactions and, therefore, the competition between the different types of magnetic exchange interactions in governing the structural behavior of these compounds upon pressure application. In other words, it appears that the volume drop at the $Fd\bar{3}m \rightarrow I4_1/amd$ transition point originates from a *spin-driven Jahn-Teller effect*. It is noteworthy that the only spinel diverging from this linear trend is $ZnCr_2Se_4$, which could serve as a potential clue for explaining its rather distinct high-pressure behavior compared to the rest of the Cr-spinels (**Figure 6**).

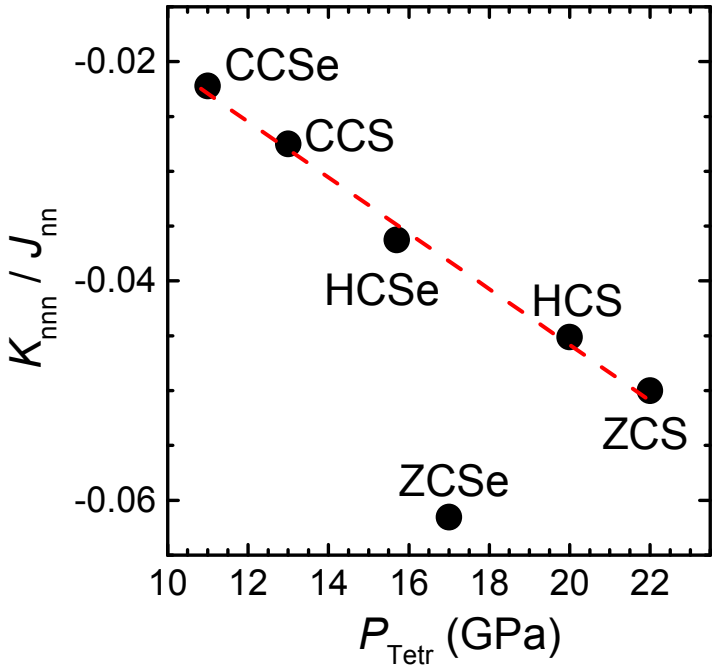

Figure 8. Plot of the magnetic exchange interaction ratio K_{nnn} / J_{nn} against the $Fd\bar{3}m \rightarrow I4_1/amd$ transition pressure P_{Tetr} for several Cr-spinels. See **Figure 6** for compound abbreviations. The K and J values are taken from Hamedoun *et al.*[75], based on the early model developed by Baltzer *et al.*[6].

Finally, we would like to comment on the apparent coexistence of a secondary phase alongside the high-pressure tetragonal and orthorhombic modifications of $ZnCr_2S_4$ (**Figure 2**). This observation is rather unique for $ZnCr_2S_4$, since such phase coexistence was not detected in any of the relevant Cr-bearing chalcogenide spinels[26–30]. Nevertheless, the coexistence of two high-pressure phases has been observed before in spinel compounds. In particular, the technologically important $LiMn_2O_4$ spinel was reported to adopt two separate tetragonal $I4_1/amd$ structures with different c/a axial ratios upon pressure increase[76]. In the case of $LiMn_2O_4$, however, such behavior was rationalized by the different ordering of the two distinct Mn^{3+} and Mn^{4+} cations present in the compound due to (partial) Li deficiency. In our case however, this scenario does not seem plausible, since any (even partial) elemental dissociation would be detected in our XRD

and Raman experiments. The identification of this secondary phase is left for future experiments employing more suitable probes, such as single-crystal XRD.

4. Conclusions

In summary, our high-pressure structural and vibrational investigations on $ZnCr_2S_4$ revealed that the starting $Fd\bar{3}m$ phase is stable up to ~22 GPa. Careful analysis of the structural parameters, however, revealed a previously unnoticed subtle *isostructural* transition between 9 and 14 GPa, which appears to be related to an electronic transition. The latter is evidenced by an abrupt drop of the overall Raman intensity, which is a common trend among Cr-bearing chalcogenide spinels under pressure[26–30]. Similar isostructural-electronic transitions were also discovered for $HgCr_2S_4$ and $ZnCr_2Se_4$ spinels, implying the possibility of modifying the physical-chemical properties of these systems upon moderate compression.

Further compression induces two reversible structural transitions at 22 and 33 GPa. The first high-pressure phase is identified as a tetragonal $I4_1/amd$ structure, whereas the second pressure-induced transition is attributed to an orthorhombic distortion of the tetragonal cell. We could also observe the development of a secondary (minority) high-pressure phase, which could not be identified in this study. A single-crystal XRD investigation on $ZnCr_2S_4$ might be able to identify this secondary high-pressure modification.

Finally, and following our previous proposal[27], we managed to unravel a direct link between the $Fd\bar{3}m \rightarrow I4_1/amd$ transition pressure and the ratio of magnetic exchange interactions active in these systems. Consequently, it appears that the tuning of the magnetic properties by external pressure can lead to first-order structural transitions toward phases of lower crystalline symmetry in these systems, i.e., sufficient compression is able to induce spin-driven Jahn-Teller transitions.

It would be interesting to investigate whether such pressure-induced magnetic modifications could explain similar structural transitions in relevant materials.

Supporting Information. Examples of Rietveld refinements, Table with the complete structural parameters for all of the high-pressure $ZnCr_2S_4$ phases, calculated d-values for the secondary (minority) high-pressure phases, calculated ZnS_4 and CrS_6 polyhedral volumes with the respective EoS fittings, Table with the Raman-related data, and a compilation of the data used in plotting **Figure 8**.

ACKNOWLEDGEMENTS

We would like to acknowledge Dr. S. Tkachev at GSECARS for his help with the DAC gas loading and Dr. D. Popov for his assistance with the XRD measurements. Portions of this work were performed at HPCAT (Sector 16), Advanced Photon Source (APS), Argonne National Laboratory. HPCAT operations are supported by DOE-NNSA under Award No. DE-NA0001974 and DOE-BES under Award No. DE-FG02-99ER45775, with partial instrumentation funding by NSF. The Advanced Photon Source is a U.S. Department of Energy (DOE) Office of Science User Facility operated for the DOE Office of Science by Argonne National Laboratory under Contract No. DE-AC02-06CH11357. Use of the COMPRES-GSECARS gas loading system was supported by COMPRES under NSF Cooperative Agreement EAR 11-57758 and by GSECARS through NSF grant EAR-1128799 and DOE grant DE-FG02-94ER14466. This research used resources of the Advanced Photon Source, a U.S. Department of Energy (DOE) Office of Science User Facility operated for the DOE Office of Science by Argonne National Laboratory under Contract No. DE-AC02-06CH11357. We are grateful to the Michigan Space Grant Consortium and the Research Faculty Fellowship of Oakland University for supporting this

research. This research has been partially supported by the Deutsche Forschungsgemeinschaft (DFG) via the Transregional Collaborative Research Center TRR 80 (Augsburg-Munich).

REFERENCES

(1) Rao, C. N. R.; Pisharody, K. P. R. Transition Metal Sulfides. *Prog. Sol. St. Chem.* **1976**, *10*, 207.

(2) Rao, C. N. R.; Raveau, B. *Transition Metal Oxides, 2nd Edition*; J. Wiley & Sons Inc., 1998.

(3) Nikiforov, K. G. Magnetically Ordered Multinary Semiconductors. *Prog. Cryst. Growth and Charact.* **1999**, *39*, 1.

(4) Yaresko, A. N. Electronic Band Structure and Exchange Coupling Constants in ACr_2X_4 Spinels (A=Zn, Cd, Hg; X=O, S, Se). *Phys. Rev. B* **2008**, *77*, 115106.

(5) Rudolf, T.; Kant, C.; Mayr, F.; Hemberger, J.; Tsurkan, V.; Loidl, A. Spin-Phonon Coupling in Antiferromagnetic Chromium Spinels. *New J. Phys.* **2007**, *9*, 76.

(6) Baltzer, P. K.; Wojtowicz, P. J.; Robbins, M.; Lopatin, E. Exchange Interactions in FM Cr Chalcogenide Spinels. *Phys. Rev.* **1966**, *151*, 367.

(7) Rudolf, T.; Kant, C.; Mayr, F.; Hemberger, J.; Tsurkan, V.; Loidl, A. Polar Phonons and Spin-Phonon Coupling in $HgCr_2S_4$ and $CdCr_2S_4$ Studied with Far-Infrared Spectroscopy. *Phys. Rev. B* **2007**, *76*, 174307.

(8) Rudolf, T.; Kant, C.; Mayr, F.; Hemberger, J.; Tsurkan, V.; Loidl, A. Spin-Phonon Coupling in $ZnCr_2Se_4$. *Phys. Rev. B* **2007**, *75*, 052410.

(9) Rudolf, T.; Kant, C.; F.Mayr; M.Schmidt; V.Tsurkan; Deisenhofer, J.; Loidl, A. Optical Properties of $ZnCr_2Se_4$ Spin-Phonon Coupling and Electronic d-d-like Excitations. *Eur. Phys. J. B* **2009**, *68*, 153.

(10) Hemberger, J.; Rudolf, T.; Krug von Nidda, H.-A.; Mayr, F.; Pimenov, A.; Tsurkan, V.; Loidl, A. Spin-Driven Phonon Splitting in Bond-Frustrated $ZnCr_2S_4$. *Phys. Rev. Lett.* **2006**, *97*, 087204.

(11) Gnezdilov, V.; Lemmens, P.; Pashkevich, Y. G.; Payen, C.; Choi, K. Y.; Hemberger, J.; Loidl, A.; Tsurkan, V. Phonon Anomalies and Possible Local Lattice Distortions in Giant Magnetocapacitive $CdCr_2S_4$. *Phys. Rev. B* **2011**, *84*, 045106.

(12) Yokaichiya, F.; Krimmel, A.; Tsurkan, V.; Margiolaki, I.; Thompson, P.; Bordallo, H. N.; Buchsteiner, A.; Stuesser, N.; Argyriou, D. N.; Loidl, A. Spin-Driven Phase Transitions in $ZnCr_2Se_4$ and $ZnCr_2S_4$ Probed by High-Resolution Synchrotron X-Ray and Neutron Powder Diffraction. *Phys. Rev. B* **2009**, *79*, 064423.

(13) Göbel, H. Local Lattice Distortions in Chromium Chalcogenide Spinels at Low Temperatures. *J. Magn. Magn. Mater.* **1976**, *3*, 143.

(14) Lee, S.-H.; Gasparovic, G.; Broholm, C.; Matsuda, M.; Chung, J.-H.; Kim, Y. J.; Ueda, H.; Xu, G.; Zschack, P.; Kakurai, K.; et al. Crystal Distortions in Geometrically Frustrated ACr_2O_4 (A = Zn,Cd). *J. Phys:. Cond. Matt.* **2007**, *19*, 145259.

(15) Hemberger, J.; Lunkenheimer, P.; Fichtl, R.; Krug von Nidda, H.-A.; Tsurkan, V.; Loidl, A. Relaxor Ferroelectricity and Colossal Magnetocapacitive Coupling in Ferromagnetic $CdCr_2S_4$. *Nature* **2005**, *434*, 364.

(16) Hemberger, J.; Lunkenheimer, P.; Fichtl, R.; Weber, S.; Tsurkan, V.; Loidl, A. Multiferroicity and Colossal Magneto-Capacitance in Cr-Thiospinels. *Phase Trans.* **2006**, *79*, 1065.

(17) Weber, S.; Lunkenheimer, P.; Fichtl, R.; Hemberger, J.; Tsurkan, V.; Loidl, A. Colossal Magnetocapacitance and Colossal Magnetoresistance in $HgCr_2S_4$. *Phys. Rev. Lett.* **2006**, *96*, 157202.

(18) Yamasaki, Y.; Miyasaka, S.; Kaneko, Y.; He, J.-P.; Arima, T.; Tokura, Y. Magnetic Reversal of the Ferroelectric Polarization in a Multiferroic Spinel Oxide. *Phys. Rev. Lett.* **2006**, *96*, 207204.

(19) Murakawa, H.; Onose, Y.; Ohgushi, K.; Ishiwata, S.; Tokura, Y. Generation of Electric Polarization with Rotating Magnetic Field in Helimagnet $ZnCr_2Se_4$. *J. Phys. Soc. Jpn.* **2008**, *77*, 043709.

(20) Oliveira, G. N. P.; Pereira, A. M.; Lopes, A. M. L.; Amaral, J. S.; dos Santos, A. M.; Ren, Y.; Mendonca, T. M.; Sousa, C. T.; Amaral, V. S.; Correia, J. G.; et al. Dynamic off-Centering of Cr^{3+} Ions and Short-Range Magneto-Electric Clusters in $CdCr_2S_4$. *Phys. Rev. B* **2012**, *86*, 224418.

(21) Dey, K.; Majumdar, S.; Giri, S. Ferroelectricity in Spiral Short-Range-Ordered Magnetic State of Spinel $MnCr_2O_4$: Significance of Topological Frustration and Magnetoelastic Coupling. *Phys. Rev. B* **2014**, *90*, 184424.

(22) Amiel, Y.; Rozenberg, G. K.; Nissim, N.; Milner, A.; Pasternak, M. P.; Hanfland, M.; Taylor, R. D. Intricate Relationship between Pressure-Induced Electronic and Structural Transformations in $FeCr_2S_4$. *Phys. Rev. B* **2011**, *84*, 224114.

(23) Albers, W.; Rooymans, C. J. M. High Pressure Polymorphism of Spinel Compounds. *Sol. St. Com.* **1965**, *3*, 417.

(24) Banus, M. D.; Lavine, M. C. Polymorphism in Selenospinels- A High-Pressure Phase of $CdCr_2Se_4$. *J. Sol. St. Chem.* **1969**, *1*, 109.

(25) Bouchard, R. J. Spinel to Defect NiAs Structure Transformation. *Mater. Res. Bull.* **1967**, *2*, 459.

(26) Efthimiopoulos, I. High-Pressure Structural and Spectroscopic Studies on Transition Metal Compounds. Ph.D. Dissertation, Aristotle University of Thessaloniki, Thessaloniki, Greece, 2010.

(27) Efthimiopoulos, I.; Liu, Z. T. Y.; Kucway, M.; Khare, S. V; Sarin, P.; Tsurkan, V.; Loidl, A.; Wang, Y. Pressure-Induced Phase Transitions in the $CdCr_2Se_4$ Spinel. *Phys. Rev. B* **2016**, *94*, 174106.

(28) Efthimiopoulos, I.; Yaresko, A.; Tsurkan, V.; Deisenhofer, J.; Loidl, A.; Park, C.; Wang, Y. Multiple Pressure-Induced Transitions in $HgCr_2S_4$. *Appl. Phys. Lett.* **2013**, *103*, 201908.

(29) Efthimiopoulos, I.; Yaresko, A.; Tsurkan, V.; Deisenhofer, J.; Loidl, A.; Park, C.; Wang, Y. Pressurizing the $HgCr_2Se_4$ Spinel at Room Temperature. *Appl. Phys. Lett.* **2014**, *104*, 11911.

(30) Efthimiopoulos, I.; Liu, Z. T. Y.; Khare, S. V; Sarin, P.; Tsurkan, V.; Loidl, A.; Popov, D.; Wang, Y. Structural Transition in the Magnetoelectric $ZnCr_2Se_4$ Spinel under Pressure. *Phys. Rev. B* **2016**, *93*, 174103.

(31) Tressler, R. E.; Hummel, F. A.; Stubican, V. S. Pressure-Temperature Study of Sulfospinels. *J. Amer. Ceram. Soc.* **1968**, *56*, 648.

(32) Waskowska, A.; Gerward, L.; Olsen, J. S.; Svane, A.; Vaitheeswaran, G.; Kanchana, V. High-Pressure Structural Behaviour of $Cu_{0.5}Fe_{0.5}Cr_2S_4$: An Experimental and Theoretical Study. *J. All. Comp.* **2013**, *578*, 202.

(33) Shannon, R. D.; Prewitt, C. T. Effective Ionic Radii in Oxides and Fluorides. *Acta Crystallogr. B* **1969**, *25*, 925.

(34) Ueda, H.; Ueda, Y. Pressure-Enhanced Direct Exchange Coupling Observed in Chromium Spinels. *Phys. Rev. B* **2008**, *77*, 224411.

(35) Xie, Y. M.; Yang, Z. R.; Zhang, Z. T.; Shen, C.; Li, L.; Ling, L. S.; Pi, L.; Sun, Y. P.; Zhang, Y. H. Magnetic Field and Pressure Effects on Magnetism of Bond-Frustrated $ZnCr_2S_4$. *J. Magn. Magn. Mater.* **2013**, *339*, 81.

(36) Wittlinger, J.; Werner, S.; Schulz, H. On the Amorphisation of $ZnCr_2S_4$ Spinel under High Pressure. *Phys. Chem. Miner.* **1997**, *24*, 597.

(37) Jo, Y.; Park, J.-G.; Kim, H. C.; Ratcliff II, W.; Cheong, S.-W. Pressure-Dependent Magnetic Properties of Geometrically Frustrated $ZnCr_2O_4$. *Phys. Rev. B* **2005**, *72*, 184421.

(38) Sakai, N.; Pifer, J. H. Effect of Hydrostatic Pressure on the Exchange Interactions in a Ferromagnetic Spinel $CdCr_2Se_4$. *Phys. Rev. B* **1986**, *33*, 1875.

(39) Tsurkan, V.; Zherlitsyn, S.; Felea, V.; Yasin, S.; Skourski, Y.; Deisenhofer, J.; Krug von Nidda, H.-A.; Lemmens, P.; Wosnitza, J.; Loidl, A. Magnetostructural Transitions in a Frustrated Magnet at High Fields. *Phys. Rev. Lett.* **2011**, *106*, 247202.

(40) Mao, H. K.; Xu, J.; Bell, P. Calibration of the Ruby Pressure Gauge to 800 Kbar Under Quasi-Hydrostatic Conditions. *J. Geophys. Res.* **1986**, *91*, 4673.

(41) Hammersley, A.; Svensson, S.; Hanfland, M.; Fitch, A.; Häusermann, D. Two-dimensional Detector Software: From Real Detector to Idealised Image or Two-theta Scan. *High Press. Res.* **1996**, *14*, 235.

(42) Toby, B. H. EXPGUI, a Graphical User Interface for GSAS. *J. Appl. Crystallogr.* **2001**, *34*, 210.

(43) von Dreele, R. B.; Larson, A. C. GSAS. *Los Alamos Natl. Lab. Rep. No. LAUR 86-748* **1994**.

(44) Birch, F. Finite Elastic Strain of Cubic Crystals. *Phys. Rev.* **1947**, *71*, 809.

(45) Gonzalez-Platas, J.; Alvaro, M.; Nestola, F.; Angel, R. EosFit7-GUI: A New Graphical User Interface for Equation of State Calculations, Analyses and Teaching. *J. Appl. Cryst.* **2016**, *49*, 1377–1382.

(46) Radaelli, P. G. Orbital Ordering in Transition-Metal Spinels. *New J. Phys.* **2005**, *7*, 53.

(47) Efthimiopoulos, I.; Liu, Z. T. Y.; Khare, S. V; Sarin, P.; Lochbiler, T.; Tsurkan, V.; Loidl, A.; Popov, D.; Wang, Y. Pressure-Induced Transition in the Multiferroic $CoCr_2O_4$ Spinel. *Phys. Rev. B* **2015**, *92*, 064108.

(48) Vaqueiro, P.; Kosidowski, M. L.; Powell, A. V. Structural Distortions of the Metal Dichalcogenide Units in AMo_2S_4 (A=V, Cr, Fe, Co) and Magnetic and Electrical Properties. *Chem. Mater.* **2002**, *14*, 1201.

(49) Hirai, S.; Mao, W. L. Novel Pressure-Induced Phase Transitions in Co_3O_4. *Appl. Phys. Lett.* **2013**, *102*, 041912.

(50) Errandonea, D.; Kumar, R. S.; Manjon, F. J.; Ursaki, V. V; Rusu, E. V. Post-Spinel Transformations and Equation of State in $ZnGa_2O_4$: Determination at High Pressure by in Situ X-Ray Diffraction. *Phys. Rev. B* **2009**, *79*, 024103.

(51) Arevalo-Lopez, A. M.; Santos-Garcia, A. J. Dos; Castillo-Martinez, E.; Duran, A.; Alario-Franco, M. A. Spinel to $CaFe_2O_4$ Transformation: Mechanism and Properties of β-$CdCr_2O_4$. *Inorg. Chem.* **2010**, *49*, 2827.

(52) Catti, M.; Fava, F. F.; Zicovich, C.; Dovesi, R. High-Pressure Decomposition of MCr_2O_4 Spinels (M=Mg, Mn, Zn) by Ab Initio Methods. *Phys. Chem. Miner.* **1999**, *26*, 389.

(53) Ves, S.; Schwarz, U.; Christensen, N. E.; Syassen, K.; Cardona, M. Cubic ZnS under Pressure: Optical-Absorption Edge, Phase Transition, and Calculated Equation of State. *Phys. Rev. B* **1990**, *42*, 9113.

(54) Li, C.; Ke, F.; Hu, Q.; Yu, Z.; Zhao, J.; Chen, Z.; Yan, H. Correlated Structural and Electronic Phase Transformations in Transition Metal Chalcogenide under High Pressure. *J. Appl. Phys.* **2016**, *119*, 135901.

(55) Takemura, K.; Yamawaki, H.; Fujihisa, H.; Kikegawa, T. High-Pressure X-Ray Studies of Zn at Room and Low Temperatures with a He-Pressure Medium. *High Press. Res.* **2002**, *22*, 337.

(56) Degtyareva, O.; Gregoryanz, E.; Mao, H.-K.; Hemley, R. J. Crystal Structure of Sulfur and Selenium at Pressures up to 160 GPa. *High Press. Res.* **2005**, *25*, 17.

(57) Degtyareva, O.; Hernandez, E. R.; Serrano, J.; Somayazulu, M.; Mao, H.-K.; Gregoryanz, E.; Hemley, R. J. Vibrational Dynamics and Stability of the High-Pressure Chain and Ring Phases in S and Se. *J. Chem. Phys.* **2007**, *126*, 084503.

(58) Waskowska, A.; Gerward, L.; Olsen, J. S.; Marques, M.; Contreras-Garcia, J.; Recio, J. M. The Bulk Modulus of Cubic Spinel Selenides: An Experimental and Theoretical Study. *High Press. Res.* **2009**, *29*, 72.

(59) Waskowska, A.; Gerward, L.; Olsen, J. S.; Feliz, M.; Llusar, R.; Gracia, L.; Marques, M.; Recio, J. M. High-Pressure Behaviour of Selenium-Based Spinels and Related Structures-an Experimental and Theoretical Study. *J. Phys:. Cond. Matt.* **2004**, *16*, 53.

(60) Kyono, A.; Gramsch, S. A.; Yamanaka, T.; Ikuta, D.; Ahart, M.; Mysen, B. O.; Mao, H. K.; Hemley, R. J. The Influence of the Jahn-Teller Effect at Fe^{2+} on the Structure of Chromite at High Pressure. *Phys. Chem. Miner.* **2012**, *39*, 131.

(61) Yong, W.; Botis, S.; Shieh, S. R.; Shi, W.; Withers, A. C. Pressure-Induced Phase Transition Study of Magnesiochromite ($MgCr_2O_4$) by Raman Spectroscopy and X-Ray Diffraction. *Phys. Earth Planet. Inter.* **2012**, *196–197*, 75.

(62) Lutz, H. D.; Becker, W.; Mueller, B.; Jung, M. Raman Single Crystal Studies of Spinel Type MCr_2S_4

(M=Mn, Fe, Co, Zn, Cd), MIn_2S_4 (M=Mn, Fe, Co, Ni), $MnCr_{2-x}In_{2x}S_4$ and $Co_{1-x}Cd_xCr_2S_4$. *J. Raman Spectr.* **1989**, *20*, 99.

(63) Kushwaha, A. K. Lattice Dynamics at Zone-Center of Sulphide and Selenide Spinels. *Commun. Theor. Phys.* **2008**, *50*, 1422.

(64) Julien, C. M.; Massot, M. Raman Spectroscopic Studies of Lithium Manganates with Spinel Structure. *J. Phys:. Cond. Matt.* **2003**, *15*, 3151.

(65) Malavasi, L.; Galinetto, P.; Mozzati, M. C.; Azzoni, C. B.; Flor, G. Raman Spectroscopy of AMn_2O_4 (A=Mn, Mg and Zn) Spinels. *Phys. Chem. Chem. Phys.* **2002**, *4*, 3876.

(66) Errandonea, D.; Meng, Y.; Somayazulu, M.; Häusermann, D. Pressure-Induced α-ω Transition in Titanium Metal: A Systematic Study of the Effects of Uniaxial Stress. *Phys. B* **2005**, *355*, 116–125.

(67) Errandonea, D.; Munoz, A.; Gonzalez-Platas, J. Comment on "High-Pressure X-Ray Diffraction Study of YBO_3/Eu^{3+}, $GdBO_3$, and $EuBO_3$: Pressure-Induced Amorphization in $GdBO_3$". *J. Appl. Phys.* **2014**, *115*, 216101.

(68) Klotz, S.; Chervin, J.-C.; Munsch, P.; Marchand, G. Le. Hydrostatic Limits of 11 Pressure Transmitting Media. *J. Phys. D Appl. Phys.* **2009**, *42*, 075413.

(69) Besson, J. M.; Itie, J. P.; Polian, A.; Weill, G.; Mansot, J. L.; Gonzalez, J. High-Pressure Phase Transition and Phase Diagram of Gallium Arsenide. *Phys. Rev. B* **1991**, *44*, 4214.

(70) Rabia, K.; Baldassarre, L.; Deisenhofer, J.; Tsurkan, V.; Kuntscher, C. A. Evolution of the Optical Properties of Chromium Spinels $CdCr_2O_4$, $HgCr_2S_4$, and $ZnCr_2Se_4$ under High Pressure. *Phys. Rev. B* **2014**, *89*, 125107.

(71) Guo, S.-D.; Liu, B.-G. Density-Functional-Theory Investigation of Pressure Induced Semiconductor-metal Transitions in the Ferromagnetic Semiconductor $HgCr_2Se_4$. *J. Phys.: Cond. Matt.* **2012**, *24*, 045502.

(72) Polian, A.; Gauthier, M.; Souza, S. M.; Triches, D. M.; de Lima, J. C.; Grandi, T. A. Two-Dimensional Pressure-Induced Electronic Topological Transition in Bi_2Te_3. *Phys. Rev. B* **2011**, *83*, 113106.

(73) Zhao, J.; Xu, L.; Liu, Y.; Yu, Z.; Li, C.; Wang, Y.; Liu, Z. Isostructural Phase Transition in Bismuth Oxide Chloride Induced by Redistribution of Charge under High Pressure. *J. Phys. Chem. C* **2015**, *119*, 27657–27665.

(74) Alvaro, M.; Nestola, F.; Ross, N.; Domeneghetti, M. C.; Reznitsky, L. High-Pressure Behavior of Thiospinel $CuCr_2S_4$. *Amer. Miner.* **2014**, *99*, 908–913.

(75) Hamedoun, M.; Zerhouni, A.; Rachadi, A.; Slimani, M.; Benyoussef, A. Exchange Integrals and Magnetic Properties of Mixed Chromium Spinel Systems: $Zn_{1-x}A_xCr_2X_4$ (A=Cd,Hg and X=S,Se). *Phys. Stat. Sol.(b)* **1995**, *192*, 159.

(76) Piszora, P.; Nowicki, W.; Darul, J. High-Pressure Metaelastic Properties of $Li_xMn_{3-x}O_4$ (X = 0.87, 0.94, 1.00). *J. Mater. Chem.* **2008**, *18*, 2447.

TOC Graphic

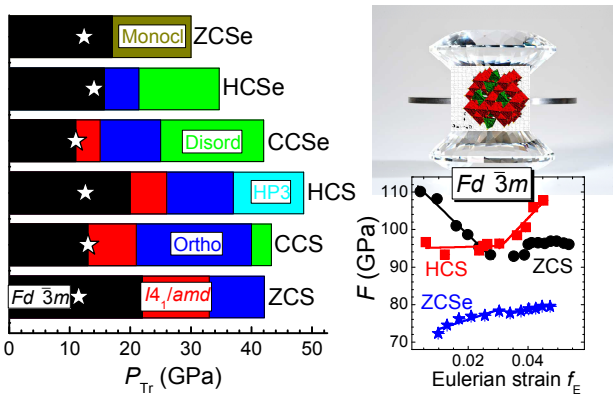
Monocl
ZCSe
HCSe
Disord
CCSe
HP3
HCS
Ortho
CCS
Fd 3̄m
I4₁/amd
ZCS
0
10
20
30
40
50
P_Tr (GPa)
Fd 3̄m
110
100
90
80
70
F (GPa)
HCS
ZCS
ZCSe
0.02
0.04
Eulerian strain f_E